DOI: 10.1002/ejic.200901006

Chemical-Bonding Assembly, Physical Characterization, and Photophysical Properties of Lanthanide Hybrids from a Functional Thiazole Bridge

Lei Guo[a] and Bing Yan*[a]

Keywords: Organic–inorganic hybrid composites / Lanthanides / Sol-gel processes / Bridging ligands / Luminescence

Two organic ligands derived from thiazole were modified by 3-(triethoxysilyl)propyl isocyanate (TESPIC) to achieve the molecular precursors (P1 and P2). Then, the organic–inorganic hybrid materials (LnM1 and LnM2, Ln = Eu and Tb) were obtained by using these as bridging molecules to coordinate with lanthanide ions and form inorganic Si–O networks with tetraethoxysilane (TEOS) after cohydrolysis and copolycondensation processes, whose composition, microstructures, and photophysical properties were studied. All of the materials were amorphous and no phase separation occurred. The photoluminescence properties of these materials revealed that all these hybrids can show the characteristic luminescence of lanthanide ions. The ratios of red/orange, decay times, emission quantum efficiency of Eu^{3+} hybrid materials were also determined. Furthermore, the number of water molecules coordinated to the Eu^{3+} ion was theoretically estimated on the basis of emission spectra and the lifetime of the $^5D_0$ state.

Introduction

Luminescent organic–inorganic hybrid materials have been widely recognized as a promising area, as they combine the thermal stability and mechanical strength of silica, together with the optical characteristics of organic active species. As we know, lanthanide(III) complexes are extensively exploited for applications such as luminescence materials, electroluminescence devices, and as fluorescence probes or labels in a variety of biological systems.[1–3] However, their applications are limited because of poor thermal stability and photostability. To circumvent these shortcomings, most of the previous studies have been focused on incorporation of luminescent molecules into silica-based sol–gel matrices.[4–8] This conventional doping method, however, seems unable to solve the problem of clustering of emitting centers because only weak interactions (such as hydrogen bonding, van der Waals forces, or weak static effects) exist between organic and inorganic moieties. As a consequence, another appealing method has emerged, which concerns covalently bonded hybrids, and the as-derived molecular-based materials exhibit excellent chemical stability and a monophasic appearance even with a high concentration of lanthanide complexes.[9–12]

Carlos et al. have done important work and have lately given a review on lanthanide-containing light-emitting organic–inorganic hybrids.[13] More recently, Binnemans gave a more extensive overview of the different types of lanthanide-based hybrid materials and compared their respective advantages and disadvantages.[14] Our research team explores covalently bonded hybrid materials in which luminescent lanthanide organic complexes are anchored to a siloxane matrix through Si–C linkages, and we have successfully exploited six paths to construct functional silylated precursors. Modification of the main groups are the amino, carboxylate, hydroxy, sulfonic, methylene, and mercapto groups.[15] After modification, we assemble the above bridge ligands with lanthanide ions and tetraethoxysilane (TEOS) to compose hybrid systems with covalent bonds. At present, the sol–gel method that is based on hydrolysis/condensation reactions has become one of the preferred synthetic routes for the development of organic–inorganic hybrids.[16–19]

On the basis of previous work, the key procedure to construct molecular-based materials is to design a functional bridging molecule by a grafting reaction; the bridge has a double function, as it coordinates to the lanthanide ions and forms a covalent Si–O network in sol–gel processing. Thiazole is a π electron-rich heterocyclic compound. Some organic ligands containing the thiazole heterocycle can be used as the lanthanide ions labeling reagent and transfer energy to the lanthanide emitter to sensitize luminescence of lanthanide ions, which can present the "antenna effects".[20] In this paper, we synthesized and characterized the organic ligands 2-amino-5-phenylthiazole (denoted L1) and 2-amino-4-phenylthiazole (denoted L2). The amino groups of organic ligands L1 and L2 possess reactive hydrogen atoms that can be expected to realize hydrogen-transfer reactions with the silane cross-linking reagent 3-(triethoxysilyl)propyl isocyanate, and the obtained silylated monomers can be used as siloxane network precursors to be in-

[a] Department of Chemistry, Tongji University,
Siping Road 1239, Shanghai 200092, China
Fax: +86-21-65982287
E-mail: byan@tongji.edu.cn

Supporting information for this article is available on the WWW under http://dx.doi.org/10.1002/ejic.200901006.

troduced into silica matrixes by Si–O bonds after hydrolysis and polycondensation processes. Finally, we obtained a series of chemically bonded lanthanide–inorganic–organic hybrid materials from a functional thiazole linkage, and the microstructures, thermal stabilities, and photoluminescence properties of the final materials were studied in detail.

Results and Discussion

As detailed in the Experimental Section, ^{1}H NMR spectra relative to the organic ligands and the silylated precursors are in full agreement with the proposed structures. The ^{1}H NMR chemical shift of the NH_2 group observed at δ = 8.73 and 8.78 ppm for L1 and L2, respectively, disappeared in the spectra of the corresponding silylated precursors, which indicates that 3-(triethoxysilyl)propyl isocyanate (TESPIC) was successfully grafted onto the organic ligand. The signal observed for the amino group attributed to the –CONH– group can further prove the grafting reaction. Furthermore, integration of the ^{1}H NMR signals corresponding to ethoxy groups shows that no hydrolysis of the precursors occurred during the grafting reaction.

Scheme 1 presents the synthesis process and the predicted structure of hybrid materials LnM1 (the synthesis of LnM2 is given in Scheme S1, Supporting Information). As we know, it is very difficult to prove the exact structures of these kinds of noncrystalline hybrid materials and even it is hardly possible to solve the coordination behavior of the lanthanide ions. However, the main composition, the coordination effects according to the lanthanide coordination chemistry principle, and the functional groups of the organic unit can be predicted. Considering the structure of the ligands in this article, we can assume that the nitrogen atom of the thiazole ring and the oxygen atom of the C=O group can coordinate with the lanthanide ions to form a stable six-membered ring structure.[21] In addition, according to the previous research of Horrocks,[22] we can deduce that two or three water molecules participate in coordination in these hybrids. These predictions have also been confirmed by infrared spectra.

The IR spectra of ligand L1, precursor P1, and hybrid material LnM1 in the 4000–400 cm^{-1} range are shown in Figure 1. From free ligand L1 (Figure 1a), the double peaks at 3384 ($\nu_{as\text{-}NH_2}$) and 3275 cm^{-1} ($\nu_{s\text{-}NH_2}$) are the unique vibrations of the NH_2 group. In Figure 1b, clear and strong evidence of nucleophilic attack of the amino group of the ligand over the isocyanate group (–N=C=O of the TESPIC molecule) is that the bands at 2268 and 859 cm^{-1} assigned to the normal and deformation vibrations of the isocyanate group disappear after a reaction time of 18 h.[23] At the same time, the band at 1667 cm^{-1} can be assigned to the C=O groups; this is proof of the formation of a –CONH group, which bonds the ligand to the propyl group of TESPIC. Additionally, two adjacent peaks at 2933 and 2882 cm^{-1} in Figure 1b are $\nu_{as}(CH_2)$ and $\nu_s(CH_2)$ of the three methylene groups of TESPIC. Furthermore, it is also found that the stretching vibration of Si–C located at 1199 cm^{-1} and the stretching vibration of Si–O at 1100 and 1041 cm^{-1}, which exist in the precursor, indicate the absorption of the siloxane bonds.

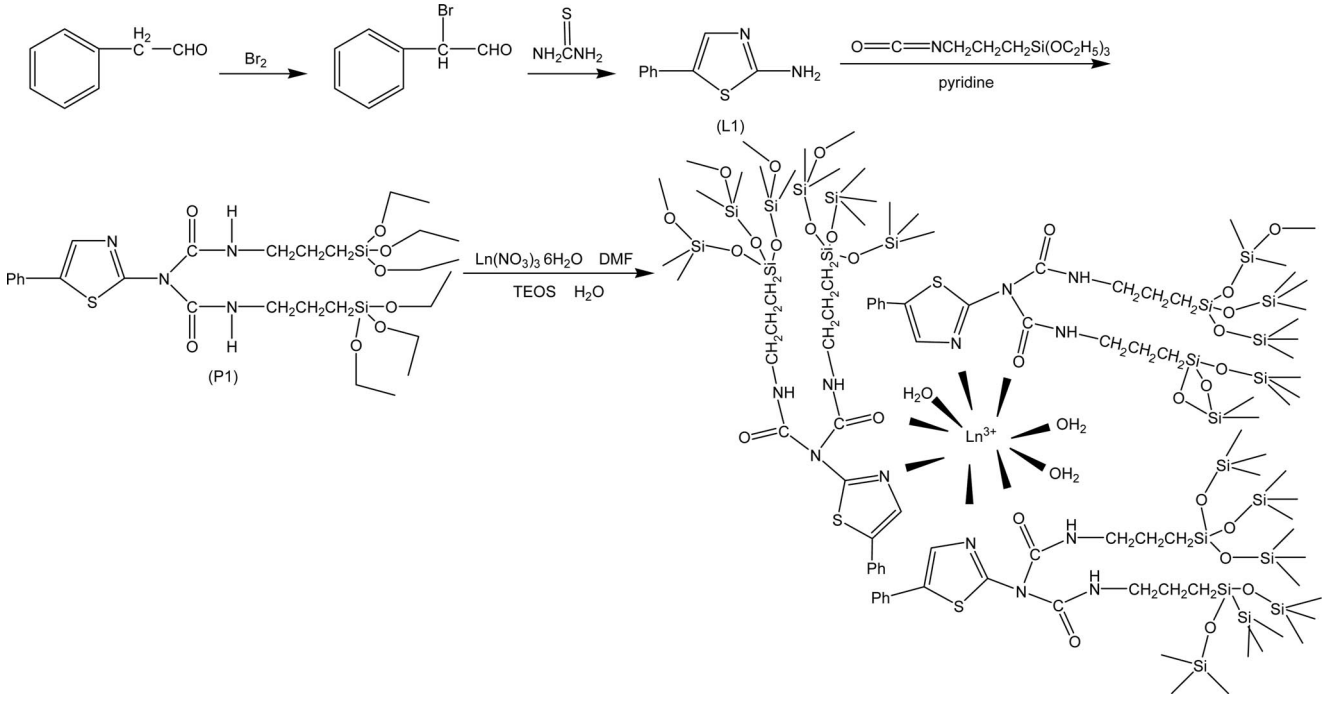

Scheme 1. Synthesis of organic ligand L1 and silylated precursor P1, and the predicted structure of hybrid materials LnM1 (Ln = Eu, Tb).

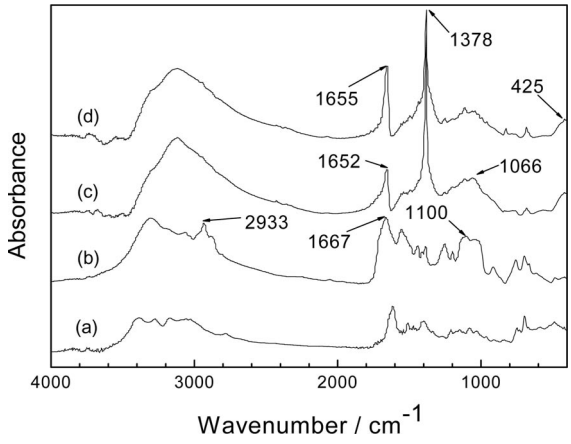

Figure 1. Fourier transform infrared spectra of (a) ligand L1, (b) precursor P1, and hybrid materials (c) EuM1 and (d) TbM1.

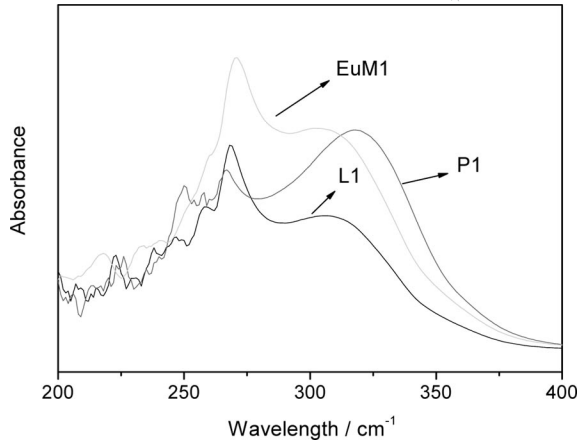

Figure 2. Ultraviolet absorption spectra of organic ligand L1, precursor P1, and hybrid material EuM1 (in DMF solution).

The IR spectra of EuM1 and TbM1 can be seen in Figure 1 (c and d, respectively). There are similar spectra of these hybrid materials with different lanthanide ions. After coordination with lanthanide ions, the ν(C=O) vibrations are shifted to lower frequencies ($\Delta\nu$ = 12–19 cm^{-1}) compared with those of P1, which can indicate complexation of the lanthanide ions with the oxygen atom.[24] The decrease in the C=N bending frequencies (from ≈1558 to ≈1540 cm^{-1}) is proof that the nitrogen atom of the thiazole ring coordinates to the lanthanide ions.[7,21] Besides, the spectra of the hybrid material indicate the formation of the Si–O–Si framework, which is evidenced by the broad bands located at about 1112–1062 cm^{-1} [ν_{as}(Si–O)]. This is attributed to hydrolysis and condensation reactions.[4,25] A strong absorption at 1378 cm^{-1} is observed for each hybrid and is assigned to a free nitrate ion.[26] A ν(O–H) vibration around 3200 cm^{-1} can be observed, which exemplifies the existence of H_2O molecules, and the $\rho_\omega(H_2O)$ stretching vibration at 425 cm^{-1} provides further evidence for the participation of water molecules in coordination in these hybrids.[27]

Figure 2 exhibits the ultraviolet absorption spectra (DMF as solvent) of L1, P1, and EuM1. From the spectra, we can see that there are two major peaks, and the peak value of the sharp peak (266 nm, π–π*) is higher than that of the broad peak (306 nm, n–π*) in the spectrum of L1. In comparison to the spectrum of P1, the peak value of the sharp peak (267 nm) is much lower than that of the broad peak (318 nm), and the broad peak experiences an obvious redshift (about 12 nm). It is estimated that TESPIC was grafted onto L1 and that covalent chemical bonds were formed successfully. After the coordination reaction, the absorption spectra of hybrid material EuM1 is a little different from that of P1. The broad peak at about 318 nm in P1 shifts to 305 nm, suggesting the energy difference among the electron transitions increased and that the coordination process with europium ions was accomplished.[28]

The room-temperature X-ray diffraction patterns of the hybrid materials in Figure S1 reveal that all the materials with $10 \leq 2\theta \leq 70°$ are totally amorphous. All diffraction curves show a similar broad peak centered around 22°, which is known as an "amorphous hump" and is a typical characteristic of amorphous silica backbone materials.[29] According to the literature,[30] for amorphous solids, the position of the first sharp diffraction peak (FSDP) can be related through a reciprocal relation to a distance in real space between the structural units (Bragg law: $2d\sin\theta = n\lambda$). We can calculate that the structural unit distance is approximately 4.04 Å. This value is similar to those reported for vitreous SiO_2, that is, 4.2 Å. The small narrow peaks in the XRD figure can be due to the incompleteness of the hydrolysis/condensation reactions between the excess amount of TEOS. However, the intension of these narrow peaks is very weak, which indicates that the content of these simple Si–O components is small. Moreover, none of the hybrid materials contain measurable amounts of phases corresponding to the pure organic compound or free Ln nitrate, which is an initial indication for the formation of the true covalently bonded molecular hybrid materials.[31]

To investigate the thermal stabilities of the obtained hybrids, thermogravimetric (TG) and differential scanning calorimetry (DSC) were performed on all of the amorphous materials. Figure 3 presents the TG, DSC, and DTG curves of TbM2 conducted at a heating rate of 5.0 °C/min. From the TG curve we can see that, from the beginning to about 175 °C, there is a mass decrease (5.99%). It is deduced that the adsorbed water and residual solvent evaporated, without any decomposition of the chemical bonds.[32] As the temperature exceeds 200 °C, the complex begins to decompose. The whole mass loss may be explained by the thermal instability of the organic parts. Related to this, the DSC curve shows that there is an obvious endothermic peak at 285.4 °C. Similar thermal behaviors are observed for other hybrid materials. Therefore, we can infer that all the materials in this article have the same structure.

The scanning electron micrographs (SEM) of the lanthanide hybrid materials demonstrate that homogeneous materials were obtained (Figure 4). On the surface of those materials, there are many linear stripes. Moreover, new small branches emerge at the end of each dendritic stripe, and the stripes will continue to grow according to the direc-

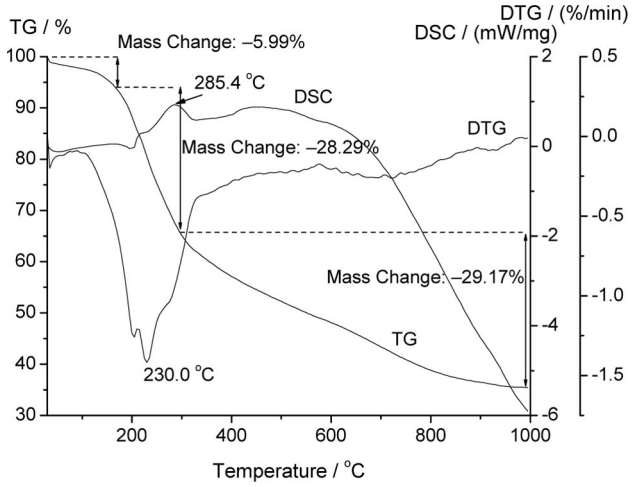

Figure 3. TG, DSC, and DTG curves of the TbM2 hybrid material.

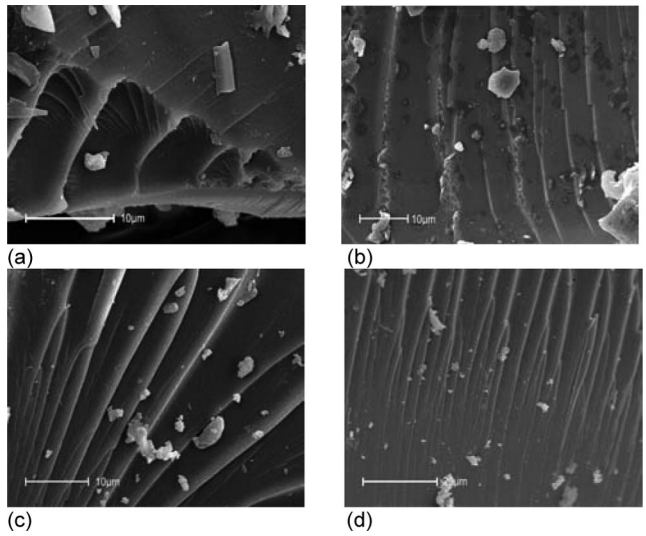

Figure 4. Scanning electron micrographs (SEM) of the hybrid materials: (a) EuM1, (b) TbM1, (c) EuM2, and (d) TbM2.

tions of these branches to form the final structure. It is indicated that the tendency to form the polymeric Si–O–Si network has become the primary tendency when it competes with the tendency to form a 1D chain-like structure, which is aroused by the complexation of the lanthanide ions. Furthermore, the microstructures of these materials are the same, suggesting that they have the same coordination behavior, and a self-assembly process might occur during the polymerization reaction. Subsequently, a complicated huge molecular system is obtained containing a functional bridge ligand with strong covalent bonds between the inorganic and organic phases. The similar self-assembly process also illustrates that the different structures of the organic ligands (L1 and L2) and the different lanthanide ions seem to have little influence on the microstructure in this hybrid system. The conditions of sol–gel processing may be the key to the formation of the microstructure and micromorphology. In addition, in comparison to hybrid materials with doped lanthanide complexes generally experiencing phase separation phenomena, the two phases in these molecular-based hybrids with chemical covalent bonds can exhibit their distinct properties together.

The characterization of diffuse reflectance absorption spectra for all the hybrid materials was carried out on powdered materials. It was observed that the spectra of the hybrid materials are similar (Figure S2, Supporting Information), which exhibit a broad absorption band in the UV/Vis range. This band also partially overlaps with the luminescence excitation spectra of LnM hybrid materials. The excitation and emission spectra of the resulting hybrid materials were measured in the solid state at room temperature (Figures 5 and 6). The excitation spectra were obtained by monitoring the emission of Eu^{3+} or Tb^{3+} at 613 or 545 nm (Figure S3, Supporting Information). For the Eu^{3+} hybrid materials, the excitation spectra are dominated by a peak centered at 394 and 393 nm, which is ascribed to the $^7F_0$–$^5L_6$ transition of Eu^{3+}, suggesting that the intramolecular energy transfer between Eu^{3+} and the organic ligands is not very good. As a result, the emission lines of the hybrid materials are assigned to the $^5D_0$–^7F_J transitions located at 589 and 614 nm for J = 1 and 2, respectively. In addition, a broad band in the blue–green spectral region can be ascribed to the emitting levels of the hybrid host.[33]

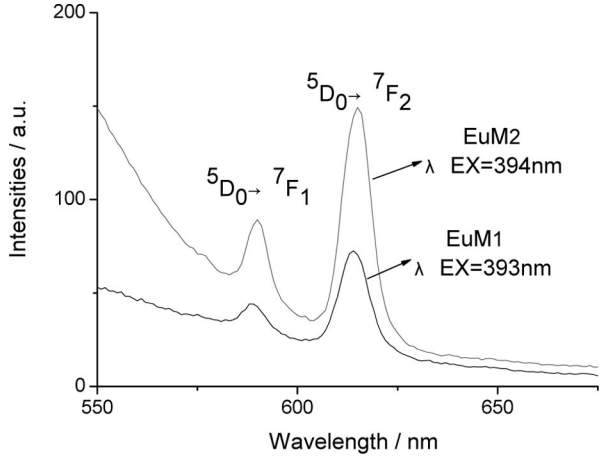

Figure 5. The emission spectra of the europium hybrid materials.

Among the red luminescence intensities, that of the $^5D_0$–$^7F_2$ transition is the strongest. The $^5D_0$–$^7F_2$ transition is an induced electric dipole transition (a hypersensitive transition); it can be detected as a relatively strong peak when Eu^{3+} does not lie in the centrosymmetric ligand field. The $^5D_0$–$^7F_1$ transition is a magnetic dipole transition, and its luminescence intensity becomes the most intensive only when the Eu^{3+} ion is the center of inversion.[34] Also, the intensity ratio of the two lines ($^5D_0$–$^7F_2$/$^5D_0$–$^7F_1$) is about 4.45 and 4.56, which indicates that the lanthanide ion is not at the center of an asymmetric coordination field. At the same time, we can see that the hybrid materials from different ligands have the same structure, which is consistent with previous conclusions. For Tb^{3+} hybrids, a band centered around 306 nm is observed in the excitation spectra, and as a result, the emission lines are assigned to the $^5D_4$–

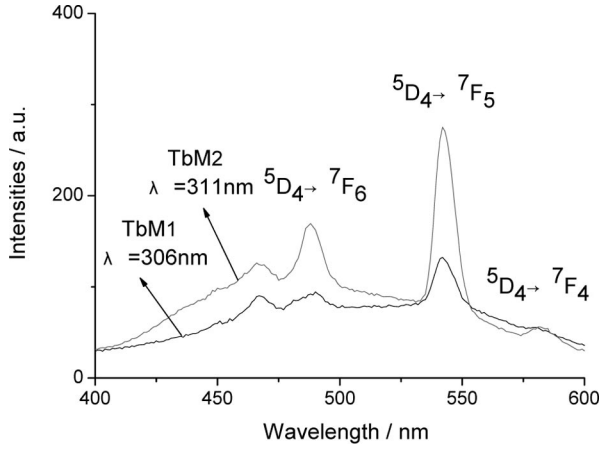

Figure 6. The emission spectra of the terbium hybrid materials.

^7F_J transitions located at 488 and 542 nm for $J = 6$ and 5, respectively. The most striking green fluorescence ($^5D_4$–$^7F_5$) is observed as a result of the fact that this emission is the most intense one.

β-Diketones, aromatic carboxylic acids, and heterocyclic ligands are already known to be good chelating groups to sensitize luminescence of lanthanide ions, and the luminescent mechanism is an intramolecular energy transfer from the ligands to the metal ions under excitation by near ultraviolet light, that is, the "antenna effect".[20a] In general, the energy transfer mechanisms between donor and acceptor species have been treated within the framework of the classic Förster[35] and Dexter[36] approaches. Whereas the Dexter model considers short-range exchange interactions, the Förster model takes multipolar long range interactions into account. According to the literature, L. D. Carlos et al. have done some work aimed at a quantitative discussion of the energy transfer mechanisms occurring in Ln^{3+}-containing organic–inorganic hybrids.[13,33] There are three distinct energy transfer pathways that can be figured out: (i) the emitting centers of the hybrid host transfer energy to the ligand excited states (hybrid-to-ligand energy transfer) or (ii) the emitting centers of the hybrid host transfer energy directly to the Ln^{3+} ions (hybrid-to-Ln^{3+} energy transfer), and (iii) the excited ligand states transfer energy to the Ln^{3+} ions (ligand-to-Ln^{3+} energy transfer). In this article, a broad band in the blue–green spectral region, which is ascribed to the emitting levels of the hybrid host and already observed in similar organic–inorganic hybrids,[37] results from a convolution of the emission originating in the NH/C=O groups of the urea bridges with electron hole recombinations occurring in the siloxane nanoclusters.

To further investigate the luminescence efficiency and to compare the influence of different ligands of these hybrid materials, the typical decay curve of the europium and terbium hybrid materials were measured, and they can be described as a single exponential $\{\mathrm{Ln}[S_{(t)}/S_0] = -k_1t = -t/\tau\}$, indicating that all Ln^{3+} ions occupy the same average coordination environment. The resulting lifetime data of europium and terbium hybrid materials are given in Table 1.

Table 1. The luminescence data of the hybrid materials.

Hybrid	EuM1	TbM1	EuM2	TbM2
I_{02}/I_{01}	4.45		4.56	
A_{exp} [s^{-1}]	2890		2137	
A_{rad} [s^{-1}]	263		269	
τ [ms]	0.346	0.302	0.468	0.406
η [%]	9.1		12.6	
n_W	≈3		≈2	

The quantum efficiency of the luminescence step, η, expresses how well the radiative processes (characterized by rate constant A_r) compete with nonradiative processes [overall rate constant A_{nr}; Equation (1)].

$$\eta = A_r/(A_r + A_{nr}) \quad (1)$$

On the basis of the emission spectra and lifetimes of the $^5D_0$ emitting level, we selectively determined the emission quantum efficiencies of the $^5D_0$ excited state of the europium ion for Eu^{3+} hybrids.[38] According to the literature,[31] the value η mainly depends on the values of two quanta: one is lifetime and the other is I_{02}/I_{01} (red/orange ratio). If the lifetimes and red/orange ratio are large, the quantum efficiency must be high. From Table 1, the red/orange ratios of these hybrids are similar, so the lifetimes of the obtained hybrids are the key to decide the quantum efficiency. Therefore, the EuM2 hybrid material has a quantum efficiency that is a little higher than the value of EuM1. In order to better express the luminescence properties of the obtained hybrids, we prepared europium and terbium complexes derived from a thiazole–imide ligand and compared their luminescence properties with those of the obtained hybrid materials. The results show that the quantum efficiency of the obtained europium materials (9.1%) is better than that of the complexes derived from a thiazole–imide ligand (6.9%), which indicates that the incorporation of the complex into these hybrid hosts can sensitize the luminescence properties of these hybrid systems. The result can be seen in Table S1 and Figure S4 (Supporting Information). Furthermore, we also compare the luminescent properties of these hybrids with those of some other hybrid materials reported in the literature (Table S2, Supporting Information).[15e,31,39] The comparisons reveal that the hybrids in this work possess a relatively long lifetime and high quantum efficiency. In addition, it is worthy to note that the absolute luminescence quantum efficiency data should be accurately performed with an integrating sphere and a calibrated detector setup for solid materials.[13] In this article, we only want to compare the photoluminescent behaviors of different hybrid materials, so the relative comparison by using a calculated value from the lifetime and emission spectra is convenient and feasible. Certainly, the relative values of the luminescent quantum efficiencies may be higher than the absolute values, because they only originate from the lifetime and spectrum.

In order to elucidate the negative influence of vibration caused by the water molecules and to further study the coordination environment surrounding the rare earth ions in

the hybrid materials, we further selectively estimated the number of coordination molecules for Eu hybrid material systems. According to the previous research of Horrocks,[22,40] the probable number of coordinated water molecules (n_w) can be determined by Equation (2).

$$n_w = 1.05A_{nr} \quad (2)$$

On the basis of the results, the coordination number of water molecules (Eu-containing hybrid materials) can be estimated to be two or three. The coordinated water molecules produce the severe vibration of the hydroxy group, resulting in a large nonradiative transition and a decrease in the luminescent efficiency.

Conclusions

In summary, four luminescent organic–inorganic hybrid materials LnM1–LnM2 were prepared by using a bridge molecule that can both coordinate to lanthanide ions (Eu^{3+} and Tb^{3+}) and form an inorganic Si–O network with tetraethoxysilane after cohydrolysis and copolycondensation though a sol–gel process. These materials display the connection of inorganic and organic parts on a molecular level. SEM proves that all of these hybrid materials exhibit homogeneous microstructures, suggesting the occurrence of self-assembly of the inorganic network and organic chain. Further investigation on the photoluminescence properties of these materials shows that all of these hybrids can display the characteristic luminescence of lanthanide ions. In addition, the different functional molecular bridges have little influence on the microstructures and photoluminescence properties such as luminescent lifetimes and quantum efficiencies.

Experimental Section

Materials: Lanthanide nitrates were obtained from their corresponding oxides in concentrated nitric acid. Tetraethoxysilane (TEOS) was distilled and stored under a N_2 atmosphere. All of the other reagents were analytically pure and solvents were purified according to literature procedures.

2-Amino-5-phenylthiazole (L1): A solution of bromine (16.0 g, 0.10 mol) in dichloromethane (10 mL) was slowly added to a cooled (–10 °C) solution of phenylacetaldehyde (12.0 g, 0.10 mol) in dichloromethane (25 mL). The resulting solution was allowed to come to room temperature and then warmed to reflux for 30 min. Aqueous sodium hydrogen carbonate was added to the cooled mixture, the product was extracted with dichloromethane, and the extract was dried (sodium sulfate) and concentrated in vacuo. The resulting residue, which was used directly in the next reaction, was treated with thiourea (15.2 g, 0.20 mol) and ethanol (75 mL). This mixture was heated at reflux for 2 h, cooled, and filtered, and the solid was treated with aqueous sodium hydrogen carbonate. Recrystallization from methanol/water finally afforded the product. Yield: 8.5 g (49%). M.p. 203–204 °C. $C_9H_8N_2S$ (176.24): calcd. C 61.3, H 4.54, N 15.9; found C 61.6, H 4.41, N 15.8. ^{1}H NMR (400 MHz, [D$_6$]DMSO): δ = 7.46 (s, 1 H, thiazolyl-H), 7.30–7.41 (m, J = 8.8 Hz, 5 H, Ar*H*), 8.73 (s, 2 H, NH_2) ppm. ^{13}C NMR (100 MHz, CDC1$_3$): δ = 102.5 (CH=*C*Ph), 128.5 (*m*-C_6H_5), 129.2 (*o*-C_6H_5), 129.4 (*p*-C_6H_5), 134.8 (*C*C=CH), 139.2 (*C*H-N), 170.0 (N=*C*-S) ppm. UV (DMF): λ (ε) = 268 (4800), 306 (3140) nm.

2-Amino-4-phenylthiazole (L2): To a solution of benzene (7.8 g, 0.10 mol) in dichloromethane (10 mL) was added of chloroacetyl chloride(11.3 g, 0.10 mol). After the solution was cooled in an ice bath, aluminum chloride (0.20 mol) was added in three portions. The mixture was gently heated at reflux for 5 h and then allowed to stir overnight at room temperature. After it was poured over ice, the product was extracted with diethyl ether, and the extract was dried (sodium sulfate) and filtered. The filtrate was concentrated in vacuo. A mixture of the above product (15 mmol) and thiourea (30 mmol) in ethanol (30 mL) was heated at reflux for 1 h. After the solvent was evaporated in vacuo, the residue was basified with aqueous potassium hydroxide, the product was extracted with diethyl ether, and the extract was dried (sodium sulfate). The solution was then filtered and concentrated in vacuo to give the final product. Yield: 1.4 g (54%). M.p. 146–148 °C. $C_9H_8N_2S$ (176.24): calcd. C 61.3, H 4.54, N 15.9; found C 60.9, H 4.72, N 16.1. ^{1}H NMR (400 MHz, [D$_6$]DMSO): δ = 7.95 (s, 1 H, thiazolyl-H), 7.35–7.42 (m, J = 8.8 Hz, 5 H, Ar*H*), 8.78 (s, 2 H, NH_2) ppm. ^{13}C NMR (100 MHz, CDC1$_3$): δ = 104.3 (CH=*C*Ph), 128.2 (*m*-C_6H_5), 129.0 (*o*-C_6H_5), 129.9 (*p*-C_6H_5), 135.1 (*C*C=CH), 159.7 (*C*H-N), 172.3 (N=*C*-S) ppm. UV (DMF): λ (ε) = 260 (4700), 302 (3200) nm.

Precursor P1: To a solution of L1 (2 mmol) in of pyridine (10 mL) was added 3-(triethoxysilyl)propylisocyanate (4 mmol) dissolved in pyridine (10 mL) dropwise with stirring, then the mixture was warmed at 70 °C for approximately 18 h under an argon atmosphere in a covered flask. The solvent was removed in vacuo, and the yellow oil was obtained in 96% yield. $C_{29}H_{50}N_4O_8SSi_2$ (670.98): calcd. C 51.9, H 7.45, N 8.4; found C 51.6, H 7.41, N 8.5. ^{1}H NMR (400 MHz, [D$_6$]DMSO): δ = 0.53 (t, J = 6.8 Hz, 4 H, CH_2Si), 1.12 (t, J = 6.8 Hz, 18 H, CH_3), 1.43 (m, J = 8.0 Hz, 4 H, CH_2), 3.45 (q, J = 6.4 Hz, 4 H, NHCH_2), 3.70 (q, J = 6.8 Hz, 12 H, SiOCH_2), 7.44–7.47 (t, J = 5.6 Hz, 2 H, N*H*), 7.86–7.90 (m, J = 8.8 Hz, 5 H, Ar*H*), 7.93 (s, 1 H, thiazolyl-H) ppm. ^{13}C NMR (100 MHz, CDC1$_3$): δ = 8.6 (*C*H$_2$Si), 13.7 (CH$_2$*C*H$_2$CH$_2$), 17.5 (*C*H$_3$CH$_2$), 48.7 (NH*C*H$_2$), 53.2 (*C*H$_2$CH$_3$), 101.2 (CH=*C*Ph), 127.1 (*m*-C_6H_5), 128.5 (*o*-C_6H_5), 129.0 (*p*-C_6H_5), 136.2 (*C*C=CH), 143.2 (*CH*-N), 156.0 (*C*=O), 168.4 (N=*C*-S) ppm. UV (DMF): λ (ε) = 267 (4220), 318 (5100) nm.

Precursor P2: Synthesized by the same manner as that given for P1, except 3-(triethoxysilyl)propyl isocyanate was treated with L2. Clear yellow oil. Yield: 95%. $C_{29}H_{50}N_4O_8SSi_2$ (670.98): calcd. C 51.9, H 7.45, N 8.4; found C 51.8, H 7.47, N 8.2. ^{1}H NMR (400 MHz, [D$_6$]DMSO): δ = 0.51 (t, J = 6.8 Hz, 4 H, CH_2Si), 1.13 (t, J = 6.8 Hz, 18 H, CH_3), 1.45 (m, J = 8.0 Hz, 4 H, CH_2), 3.50 (q, J = 6.4 Hz, 4 H, NHCH_2), 3.90 (q, J = 6.8 Hz, 12 H, SiOCH_2), 8.42–8.46 (t, J = 5.6 Hz, 2 H, N*H*), 7.92–7.95 (m, J = 8.8 Hz, 5 H, Ar*H*), 8.85 (s, 1 H, thiazolyl-H) ppm. ^{13}C NMR (100 MHz, CDC1$_3$): δ = 7.9 (*C*H$_2$Si), 13.4 (CH$_2$*C*H$_2$CH$_2$), 16.8 (*C*H$_3$CH$_2$), 45.3 (NH*C*H$_2$), 51.2 (*C*H$_2$CH$_3$), 102.8 (C=*C*HS), 128.2 (*m*-C_6H_5), 128.9 (*o*-C_6H_5), 129.1 (*p*-C_6H_5), 136.4 (*C*C=CH), 151.8 (CH=*C*Ph), 155.3 (*C*=O), 174.4 (N=*C*-S) ppm. UV (DMF): λ (ε) = 262 (4300), 320 (3150) nm.

Synthesis of the Molecular Hybrid Materials Containing Lanthanide (LnM1 and LnM2, Ln = Eu and Tb) through a Sol-Gel Procedure: Precursor P1 or P2 was dissolved in DMF and a stoichiometric amount of Ln(NO$_3$)·6H$_2$O was added to the stirring mixture. After 3 h, TEOS and H$_2$O were added with stirring, and then one drop of diluted hydrochloric acid was added to promote hydrolysis. The mol ratio of Ln(NO$_3$)·6H$_2$O/Pn/TEOS/H$_2$O was 1:3:6:24. After the

hydrolysis, an appropriate amount of hexamethylenetetramine was added to adjust to pH 6–7. The resulting mixture was agitated magnetically to achieve a single phase, and thermal treatment was performed at 60 °C in a covered Teflon beaker for about 6–7 d until the sample solidified. The obtained materials were washed with ethanol and dried at 70 °C for 2 d. The final molecular hybrid materials were collected as monolithic bulks and were ground into powdered material for the photophysical studies. In order to compare the luminescent properties of the hybrids, we also synthesize the lanthanide complexes with P1 and P2 by homogeneous precipitation. $Eu(P1)_3{\cdot}2H_2O$ (2200.94): calcd. C 47.4, H 7.00, N 7.61; found C 47.1, H 6.78, N 7.31. $Tb(P1)_3{\cdot}2H_2O$(2207.94): calcd. C 47.3, H 6.97, N 7.60; found C 47.0, H 6.74, N 7.37. $Eu(P2)_3{\cdot}2H_2O$ (2200.94): calcd. C 47.4, H 7.00, N 7.61; found C 47.1, H 6.81, N 7.33. $Tb(P2)_3{\cdot}2H_2O$ (2207.94): calcd. C 47.3, H 6.97, N 7.60; found C 47.2, H 6.77, N 7.42.

Characterization: Fourier transform infrared spectra were recorded on KBr disks by using a Nicolet model 5SXC spectrometer in the 4000–400 cm^{-1} region. ^1H NMR spectra were measured by with a Bruker Avance-400 spectrometer with tetramethylsilane (TMS) as internal reference ([D_6]DMSO as solvent). The ultraviolet absorption spectra (5×10^{-4} M DMF solution) and the ultraviolet-visible diffuse reflection spectra of the powder samples were recorded with an Agilent 8453 spectrophotometer and a BWS003 spectrophotometer, respectively. Melting points were measured with a XT4–100XA apparatus. The X-ray diffraction (XRD) measurements were carried out on powdered samples with a Bruker D8 diffractometer (40 mA/40 kV) by using monochromated Cu-$K_{\alpha 1}$ radiation (λ = 1.54 Å) over the 2θ range from 10 to 70°. Differential scanning calorimetry (DSC) and thermogravimetric analysis (TGA) were performed with a Netzsch STA 449C with a heating rate of 5 °C/min under a nitrogen atmosphere. Scanning electronic microscope (SEM) images were obtained with a Philips XL-30. Fluorescence excitation and emission spectra were obtained with a Shimadzu RF-5301 spectrofluorimeter at room temperature. Luminescent lifetimes were recorded with an Edinburgh Instruments FLS 920 phosphorimeter by using a 450 W xenon lamp as the excitation source (pulse width, 3 μs).

Supporting Information (see footnote on the first page of this article): Luminescence data for europium and terbium complexes derived from a thiazole–imide ligand and some other europium organic–inorganic hybrids; scheme of the synthesis process; X-ray diffraction graph of hybrid materials; ultraviolet-visible diffuse reflection absorption spectra and excitation spectra of the hybrid materials; emission spectra of the complexes derived from a thiazole–imide ligand.

Acknowledgments

This work was supported by the National Natural Science Foundation of China (20971100) and the Program for New Century Excellent Talents in University (NCET-08-0398).

[1] a) G. E. Buono-core, H. Li, B. Marciniak, *Coord. Chem. Rev.* **1990**, *90*, 55–87; b) X. Q. Song, J. R. Zheng, W. S. Liu, Z. H. Ju, *Spectrochim. Acta A* **2008**, *69*, 49–55; c) W. N. Wu, N. Tang, L. Yan, *J. Fluoresc.* **2008**, *18*, 101–107.

[2] a) A. Edward, T. Y. Chu, C. Claude, I. Sokolik, Y. Okamoto, R. Dorsinville, *Synth. Met.* **1997**, *84*, 433–434; b) J. Kido, K. Nagai, Y. Okamoto, *J. Alloys Compd.* **1993**, *192*, 30–33; c) J. B. Yu, L. Zhou, H. J. Zhang, Y. X. Zheng, H. R. Li, R. P. Deng, Z. P. Peng, Z. F. Li, *Inorg. Chem.* **2005**, *44*, 1611–1618.

[3] a) F. B. Wu, C. Zhang, *Anal. Biochem.* **2002**, *311*, 57–67; b) T. Nishioka, J. L. Yuan, Y. J. Yamamoto, K. Sumitomo, Z. Wang, K. Hashino, C. Hosoya, K. Ikawa, G. L. Wang, K. Matsumoto, *Inorg. Chem.* **2006**, *45*, 4088–4096; c) S. L. Klakamp, W. D. Horrocks, *J. Inorg. Biochem.* **1992**, *46*, 193–205.

[4] A. C. Franville, R. Mahiou, D. Zambon, J. C. Cousseins, *Solid State Sci.* **2001**, *3*, 211–212.

[5] H. R. Li, J. Lin, H. J. Zhang, L. S. Fu, Q. G. Meng, S. B. Wang, *Chem. Mater.* **2002**, *14*, 3651–3655.

[6] C. Sanchez, B. Lebeau, F. Chaput, J. P. Boilot, *Adv. Mater.* **2003**, *15*, 1969–1994.

[7] N. Lin, H. R. Li, Y. G. Wang, Y. Feng, D. S. Qin, Q. Y. Gan, S. D. Chen, *Eur. J. Inorg. Chem.* **2008**, 4781–4785.

[8] X. M. Guo, X. M. Wang, H. J. Zhang, L. S. Fu, H. D. Guo, J. B. Yu, L. D. Carlos, K. Y. Yang, *Microporous Mesoporous Mater.* **2008**, *116*, 28–35.

[9] J. Wang, H. S. Wang, F. Y. Liu, L. S. Fu, H. J. Zhang, *Mater. Lett.* **2003**, *57*, 1210–1214.

[10] H. R. Li, J. Lin, H. J. Zhang, H. C. Li, L. S. Fu, Q. G. Meng, *Chem. Commun.* **2001**, 1212–1213.

[11] I. L. V. Rose, O. A. Serra, E. J. Nassa, *J. Lumin.* **1997**, *72*, 532–534.

[12] P. C. R. Soares-Santos, H. I. S. Nogueira, V. Felix, M. G. B. Drew, R. A. S. Ferreira, L. D. Carlos, *Chem. Mater.* **2003**, *15*, 100–108.

[13] L. D. Carlos, R. A. S. Ferreira, V. D. Bermudez, J. L. S. Ribeiro, *Adv. Mater.* **2009**, *21*, 509–534.

[14] K. Binnemans, *Chem. Rev.* **2009**, *109*, 4283–4374.

[15] a) Q. M. Wang, B. Yan, *J. Mater. Chem.* **2004**, *14*, 2450–2455; b) Q. M. Wang, B. Yan, *Inorg. Chem. Commun.* **2004**, *7*, 747–750; c) Q. M. Wang, B. Yan, *Cryst. Growth Des.* **2005**, *5*, 497–503; d) H. F. Lu, B. Yan, *J. Non-Cryst. Solids* **2006**, *352*, 5331–5336; e) B. Yan, H. F. Lu, *Inorg. Chem.* **2008**, *47*, 5601–5611; f) B. Yan, Q. M. Wang, *Cryst. Growth Des.* **2008**, *8*, 1484–1489.

[16] U. Narang, R. Wang, P. Prasad, F. Bright, *J. Phys. Chem.* **1994**, *98*, 17–22.

[17] R. Corriu, D. Leclercq, *Angew. Chem. Int. Ed. Engl.* **1996**, *35*, 1420–1436.

[18] B. Lebeau, C. E. Fowler, S. R. Hall, *J. Mater. Chem.* **1999**, *9*, 2279–2285.

[19] U. Schubert, N. Husing, A. Lorenz, *Chem. Mater.* **1995**, *7*, 2010–2027.

[20] a) J. M. Lehn, *Angew. Chem. Int. Ed. Engl.* **1990**, *29*, 1304–1319; b) V. M. Mukkala, P. Liitti, I. Hemmila, H. Takalo, *Helv. Chim. Acta* **1996**, *79*, 295–306; c) M. Latva, H. Takalo, V. M. Mukkala, J. Kankare, *Inorg. Chim. Acta* **1998**, *267*, 63–72.

[21] A. C. Franvillea, D. Zambona, R. Mahioua, S. Choua, Y. Troinb, J. C. Cousseinsa, *J. Alloys Compd.* **1998**, *275–277*, 831–834.

[22] W. Horrocks, W. De, D. R. Sudnick, *J. Am. Chem. Soc.* **1979**, *101*, 334–340.

[23] M. A. García-Sánchez, V. De la Luz, M. L. Estrada-Rico, M. M. Murillo-Martínez, M. I. Coahuila-Hernández, R. Sosa-Fonseca, S. R. Tello-Solís, F. Rojas, A. Campero, *J. Non-Cryst. Solids* **2009**, *355*, 120–125.

[24] A. C. Franville, D. Zambon, R. Mahiou, *Chem. Mater.* **2000**, *12*, 428–435.

[25] E. Pretsch, P. Buhlmann, C. Affolter (Eds.), *Structure Determination of Organic Compounds*, 2nd printing, Springer, Berlin, **2003**.

[26] B. Klingenberg, M. A. Vannice, *Chem. Mater.* **1996**, *8*, 2755–2768.

[27] K. Nakamoto, *Infrared and Raman Spectra of Inorganic Coordination Compound* (translated by D. R. Huang), Chemical Industry Press, Beijing, **1986**, pp. 252–254.

[28] X. F. Qiao, B. Yan, *Inorg. Chem.* **2009**, *48*, 4714–4723.

[29] M. C. Goncalves, V. D. Bermudez, R. A. S. Ferreira, L. D. Carlos, D. J. Ostrovskii, J. Rocha, *Chem. Mater.* **2004**, *16*, 2530–2543.

[30] a) L. D. Carlors, V. D. Bermudez, R. A. Sa Ferreira, L. Marques, M. Assuncao, *Chem. Mater.* **1999**, *11*, 581–588; b) S. C. Moss in *Physics of Disorder Materials* (Eds.: D. Adler, H. Fritzche, S. Ovshinsky), Plenum Press, New York, **1985**.
[31] a) J. L. Liu, B. Yan, *J. Phys. Chem. C* **2008**, *112*, 14168–14178; b) J. L. Liu, B. Yan, *J. Phys. Chem. B* **2008**, *112*, 10898–10907.
[32] G. Xu, Z. M. Wang, Z. He, *Inorg. Chem.* **2002**, *41*, 6802–6807.
[33] P. P. Lima, S. S. Nobre, R. O. Freire, S. A. Júnior, R. A. S. Ferreira, U. Pischel, O. L. Malta, L. D. Carlos, *J. Phys. Chem. C* **2007**, *111*, 17627–17634.
[34] Q. Su, *Chemistry of Rare Earths*, Henan Technology & Science Press, Zhengzhou, **1993**, p. 304.
[35] T. Z. Förster, *Z. Naturforsch.* **1949**, *4a*, 321–327.
[36] D. L. Dexter, *J. Chem. Phys.* **1953**, *21*, 836–850.
[37] a) L. D. Carlos, R. A. S. Ferreira, V. D. Bermudez, S. J. L. Ribeiro, *Adv. Funct. Mater.* **2001**, *11*, 111–115; b) R. A. S. Ferreira, L. D. Carlos, V. D. Bermudez, C. Molina, K. Dahmouche, Y. Messaddeq, S. J. L. Ribeiro, *J. Sol-Gel Sci. Technol.* **2003**, *26*, 315–319; c) L. D. Carlos, V. D. Bermudez, V. S. Amaral, S. C. Nunes, N. J. O. Silva, R. A. S. Ferreira, J. Rocha, C. V. Santilli, D. Ostrovskii, *Adv. Mater.* **2007**, *19*, 341–348.
[38] a) M. H. V. Werts, R. T. F. Jukes, J. W. Verhoeven, *Phys. Chem. Chem. Phys.* **2002**, *4*, 1542–1548; b) E. E. S. Teotonio, J. G. P. Espinola, H. F. Brito, O. L. Malta, S. F. Oliveria, D. L. A. de Faria, C. M. S. Izumi, *Polyhedron* **2002**, *21*, 1837–1844; c) O. L. Malta, M. A. C. dosSantos, L. C. Thompson, N. K. Ito, *J. Lumin.* **1996**, *69*, 77–84; d) G. F. de Sa, O. L. Malta, C. D. Donega, A. M. Simas, R. L. Longo, P. A. Santa-Cruz, E. F. da Silva, *Coord. Chem. Rev.* **2000**, *196*, 165–195; e) J. C. Boyer, F. Vetrone, J. A. Capobianco, A. Speghini, M. Bettinelli, *J. Phys. Chem. B* **2004**, *108*, 20137–20143.
[39] H. F. Lu, B. Yan, J. L. Liu, *Inorg. Chem.* **2009**, *48*, 3966–3975.
[40] a) P. Tien, L. K. Chau, *Chem. Mater.* **1999**, *11*, 2141–2147; b) S. S. Nobre, P. P. Lima, L. Mafra, R. A. S. Ferreira, R. O. Freire, L. S. Fu, U. Pischel, V. D. Bermudez, O. L. Malta, L. D. Carlos, *J. Phys. Chem. C* **2007**, *111*, 3275–3284.

Received: October 15, 2009
Published Online: February 3, 2010

